

Elastic and Inelastic Photoproduction of J/ψ Mesons at HERA

H1 Collaboration

Abstract

Results on J/ψ production in ep interactions in the H1 experiment at HERA are presented. The J/ψ mesons are produced by almost real photons ($Q^2 \approx 0$) and detected via their leptonic decays. The data have been taken in 1994 and correspond to an integrated luminosity of 2.7 pb^{-1} . The γp cross section for elastic J/ψ production is observed to increase strongly with the center of mass energy. The cross section for diffractive J/ψ production with proton dissociation is found to be of similar magnitude as the elastic cross section. Distributions of transverse momentum and decay angle are studied and found to be in accord with a diffractive production mechanism. For inelastic J/ψ production the total γp cross section, the distribution of transverse momenta, and the elasticity of the J/ψ are compared to NLO QCD calculations in a colour singlet model and agreement is found. Diffractive ψ' production has been observed and a first estimate of the ratio to J/ψ production in the HERA energy regime is given.

S. Aid¹⁴, V. Andreev²⁶, B. Andrieu²⁹, R.-D. Appuhn¹², M. Arpagaus³⁷, A. Babaev²⁵,
 J. Bähr³⁶, J. Bán¹⁸, Y. Ban²⁸, P. Baranov²⁶, E. Barrelet³⁰, R. Barschke¹², W. Bartel¹²,
 M. Barth⁵, U. Bassler³⁰, H.P. Beck³⁸, H.-J. Behrend¹², A. Belousov²⁶, Ch. Berger¹,
 G. Bernardi³⁰, R. Bernet³⁷, G. Bertrand-Coremans⁵, M. Besançon¹⁰, R. Beyer¹², P. Biddulph²³,
 P. Bispham²³, J.C. Bizot²⁸, V. Blobel¹⁴, K. Borrás⁹, F. Botterweck⁵, V. Boudry²⁹, A. Braemer¹⁵,
 W. Braunschweig¹, V. Brisson²⁸, D. Bruncko¹⁸, C. Brune¹⁶, R. Buchholz¹², L. Büngener¹⁴,
 J. Bürger¹², F.W. Büsler¹⁴, A. Buniatian^{12,39}, S. Burke¹⁹, M.J. Burton²³, G. Buschhorn²⁷,
 A.J. Campbell¹², T. Carli²⁷, F. Charles¹², M. Charlet¹², D. Clarke⁶, A.B. Clegg¹⁹, B. Clerbaux⁵,
 S. Cocks²⁰, J.G. Contreras⁹, C. Cormack²⁰, J.A. Coughlan⁶, A. Courau²⁸, M.-C. Cousinou²⁴,
 G. Cozzika¹⁰, L. Criegee¹², D.G. Cussans⁶, J. Cvach³¹, S. Dagoret³⁰, J.B. Dainton²⁰,
 W.D. Dau¹⁷, K. Daum³⁵, M. David¹⁰, C.L. Davis¹⁹, B. Delcourt²⁸, A. De Roeck¹²,
 E.A. De Wolf⁵, M. Dirkmann⁹, P. Dixon¹⁹, P. Di Nezza³³, W. Dlugosz⁸, C. Dollfus³⁸,
 J.D. Dowell⁴, H.B. Dreis², A. Droutskoi²⁵, D. Düllmann¹⁴, O. Dünker¹⁴, H. Duhm¹³,
 J. Ebert³⁵, T.R. Ebert²⁰, G. Eckerlin¹², V. Efremenko²⁵, S. Egli³⁸, R. Eichler³⁷, F. Eisele¹⁵,
 E. Eisenhandler²¹, R.J. Ellison²³, E. Elsen¹², M. Erdmann¹⁵, W. Erdmann³⁷, E. Evrard⁵,
 A.B. Fahr¹⁴, L. Favart⁵, A. Fedotov²⁵, D. Feeken¹⁴, R. Felst¹², J. Feltesse¹⁰, J. Ferencei¹⁸,
 F. Ferrarotto³³, K. Flamm¹², M. Fleischer⁹, M. Flieser²⁷, G. Flügge², A. Fomenko²⁶,
 B. Fominykh²⁵, J. Formánek³², J.M. Foster²³, G. Franke¹², E. Fretwurst¹³, E. Gabathuler²⁰,
 K. Gabathuler³⁴, F. Gaede²⁷, J. Garvey⁴, J. Gayler¹², M. Gebauer³⁶, A. Gellrich¹², H. Genzel¹,
 R. Gerhards¹², A. Glazov³⁶, U. Goerlach¹², L. Goerlich⁷, N. Gogitidze²⁶, M. Goldberg³⁰,
 D. Goldner⁹, K. Golec-Biernat⁷, B. Gonzalez-Pineiro³⁰, I. Gorelov²⁵, C. Grab³⁷, H. Grässler²,
 R. Grässler², T. Greenshaw²⁰, R. Griffiths²¹, G. Grindhammer²⁷, A. Gruber²⁷, C. Gruber¹⁷,
 J. Haack³⁶, D. Haidt¹², L. Hajduk⁷, M. Hampel¹, W.J. Haynes⁶, G. Heinzelmann¹⁴,
 R.C.W. Henderson¹⁹, H. Henschel³⁶, I. Herynek³¹, M.F. Hess²⁷, W. Hildesheim¹², K.H. Hiller³⁶,
 C.D. Hilton²³, J. Hladký³¹, K.C. Hoeger²³, M. Höppner⁹, D. Hoffmann¹², T. Holtom²⁰,
 R. Horisberger³⁴, V.L. Hudgson⁴, M. Hütte⁹, H. Hufnagel¹⁵, M. Ibbotson²³, H. Itterbeck¹,
 A. Jacholkowska²⁸, C. Jacobsson²², M. Jaffre²⁸, J. Janoth¹⁶, T. Jansen¹², L. Jönsson²²,
 K. Johannsen¹⁴, D.P. Johnson⁵, L. Johnson¹⁹, H. Jung¹⁰, P.I.P. Kalmus²¹, M. Kander¹²,
 D. Kant²¹, R. Kaschowitz², U. Kathage¹⁷, J. Katzy¹⁵, H.H. Kaufmann³⁶, O. Kaufmann¹⁵,
 S. Kazarian¹², I.R. Kenyon⁴, S. Kermiche²⁴, C. Keuker¹, C. Kiesling²⁷, M. Klein³⁶,
 C. Kleinwort¹², G. Knies¹², T. Köhler¹, J.H. Köhne²⁷, H. Kolanoski³, F. Kole⁸, S.D. Kolya²³,
 V. Korbel¹², M. Korn⁹, P. Kostka³⁶, S.K. Kotelnikov²⁶, T. Krämerkämper⁹, M.W. Krasny^{7,30},
 H. Krehbiel¹², D. Krücker², U. Krüger¹², U. Krüner-Marquis¹², H. Küster²², M. Kuhlen²⁷,
 T. Kurča³⁶, J. Kurzhöfer⁹, D. Lacour³⁰, B. Laforge¹⁰, R. Lander⁸, M.P.J. Landon²¹, W. Lange³⁶,
 U. Langenegger³⁷, J.-F. Laporte¹⁰, A. Lebedev²⁶, F. Lehner¹², C. Leverenz¹², S. Levonian²⁶,
 Ch. Ley², G. Lindström¹³, M. Lindstroem²², J. Link⁸, F. Linsel¹², J. Lipinski¹⁴, B. List¹²,
 G. Lobo²⁸, H. Lohmander²², J.W. Lomas²³, G.C. Lopez¹³, V. Lubimov²⁵, D. Lüke^{9,12},
 N. Magnussen³⁵, E. Malinovski²⁶, S. Mani⁸, R. Maraček¹⁸, P. Marage⁵, J. Marks²⁴,
 R. Marshall²³, J. Martens³⁵, G. Martin¹⁴, R. Martin²⁰, H.-U. Martyn¹, J. Martyniak⁷,
 T. Mavroidis²¹, S.J. Maxfield²⁰, S.J. McMahon²⁰, A. Mehta⁶, K. Meier¹⁶, T. Merz³⁶,
 A. Meyer¹⁴, A. Meyer¹², H. Meyer³⁵, J. Meyer¹², P.-O. Meyer², A. Migliori²⁹, S. Mikocki⁷,
 D. Milstead²⁰, J. Moeck²⁷, F. Moreau²⁹, J.V. Morris⁶, E. Mroczko⁷, D. Müller³⁸, G. Müller¹²,
 K. Müller¹², P. Murín¹⁸, V. Nagovizin²⁵, R. Nahnhauser³⁶, B. Naroska¹⁴, Th. Naumann³⁶,
 P.R. Newman⁴, D. Newton¹⁹, D. Neyret³⁰, H.K. Nguyen³⁰, T.C. Nicholls⁴, F. Niebergall¹⁴,
 C. Niebuhr¹², Ch. Niedzballa¹, H. Niggli³⁷, R. Nisius¹, G. Nowak⁷, G.W. Noyes⁶, M. Nyberg-
 Werther²², M. Oakden²⁰, H. Oberlack²⁷, U. Obrock⁹, J.E. Olsson¹², D. Ozerov²⁵, P. Palmén²,
 E. Panaro¹², A. Panitch⁵, C. Pascaud²⁸, G.D. Patel²⁰, H. Pawletta², E. Peppel³⁶, E. Perez¹⁰,

J.P. Phillips²⁰, A. Pieuchot²⁴, D. Pitzl³⁷, G. Pope⁸, S. Prell¹², R. Prosi¹², K. Rabbertz¹, G. Rädcl¹², F. Raupach¹, P. Reimer³¹, S. Reinshagen¹², H. Rick⁹, V. Riech¹³, J. Riedlberger³⁷, F. Riepenhausen², S. Riess¹⁴, E. Rizvi²¹, S.M. Robertson⁴, P. Robmann³⁸, H.E. Roloff³⁶, R. Roosen⁵, K. Rosenbauer¹, A. Rostovtsev²⁵, F. Rouse⁸, C. Royon¹⁰, K. Rüter²⁷, S. Rusakov²⁶, K. Rybicki⁷, N. Sahlmann², D.P.C. Sankey⁶, P. Schacht²⁷, S. Schiek¹⁴, S. Schleif¹⁶, P. Schleper¹⁵, W. von Schlippe²¹, D. Schmidt³⁵, G. Schmidt¹⁴, A. Schöning¹², V. Schröder¹², E. Schuhmann²⁷, B. Schwab¹⁵, F. Sefkow¹², M. Seidel¹³, R. Sell¹², A. Semenov²⁵, V. Shekelyan¹², I. Sheviakov²⁶, L.N. Shtarkov²⁶, G. Siegmö¹⁷, U. Siewert¹⁷, Y. Sirois²⁹, I.O. Skillicorn¹¹, P. Smirnov²⁶, J.R. Smith⁸, V. Solochenko²⁵, Y. Soloviev²⁶, A. Specka²⁹, J. Spiekermann⁹, S. Spielman²⁹, H. Spitzer¹⁴, F. Squinabol²⁸, R. Starosta¹, M. Steenbock¹⁴, P. Steffen¹², R. Steinberg², H. Steiner^{12,40}, B. Stella³³, A. Stellberger¹⁶, J. Stier¹², J. Stiewe¹⁶, U. Stöblein³⁶, K. Stolze³⁶, U. Straumann³⁸, W. Struczinski², J.P. Sutton⁴, S. Tapprogge¹⁶, M. Taševský³², V. Tchernyshov²⁵, S. Tchetchelnitski²⁵, J. Theissen², C. Thiebaut²⁹, G. Thompson²¹, P. Truöl³⁸, J. Turnau⁷, J. Tutas¹⁵, P. Uelkes², A. Usik²⁶, S. Valkár³², A. Valkárová³², C. Vallée²⁴, D. Vandenplas²⁹, P. Van Esch⁵, P. Van Mechelen⁵, Y. Vazdik²⁶, P. Verrecchia¹⁰, G. Villet¹⁰, K. Wacker⁹, A. Wagener², M. Wagener³⁴, A. Walther⁹, B. Waugh²³, G. Weber¹⁴, M. Weber¹², D. Wegener⁹, A. Wegner²⁷, T. Wengler¹⁵, M. Werner¹⁵, L.R. West⁴, T. Wilksen¹², S. Willard⁸, M. Winde³⁶, G.-G. Winter¹², C. Wittek¹⁴, E. Wunsch¹², J. Žáček³², D. Zarbock¹³, Z. Zhang²⁸, A. Zhokin²⁵, M. Zimmer¹², F. Zomer²⁸, J. Zsembery¹⁰, K. Zuber¹⁶, and M. zurNedden³⁸ ¹ I. Physikalisches Institut der RWTH, Aachen, Germany^a

² III. Physikalisches Institut der RWTH, Aachen, Germany^a

³ Institut für Physik, Humboldt-Universität, Berlin, Germany^a

⁴ School of Physics and Space Research, University of Birmingham, Birmingham, UK^b

⁵ Inter-University Institute for High Energies ULB-VUB, Brussels; Universitaire Instelling Antwerpen, Wilrijk; Belgium^c

⁶ Rutherford Appleton Laboratory, Chilton, Didcot, UK^b

⁷ Institute for Nuclear Physics, Cracow, Poland^d

⁸ Physics Department and IIRPA, University of California, Davis, California, USA^e

⁹ Institut für Physik, Universität Dortmund, Dortmund, Germany^a

¹⁰ CEA, DSM/DAPNIA, CE-Saclay, Gif-sur-Yvette, France

¹¹ Department of Physics and Astronomy, University of Glasgow, Glasgow, UK^b

¹² DESY, Hamburg, Germany^a

¹³ I. Institut für Experimentalphysik, Universität Hamburg, Hamburg, Germany^a

¹⁴ II. Institut für Experimentalphysik, Universität Hamburg, Hamburg, Germany^a

¹⁵ Physikalisches Institut, Universität Heidelberg, Heidelberg, Germany^a

¹⁶ Institut für Hochenergiephysik, Universität Heidelberg, Heidelberg, Germany^a

¹⁷ Institut für Reine und Angewandte Kernphysik, Universität Kiel, Kiel, Germany^a

¹⁸ Institute of Experimental Physics, Slovak Academy of Sciences, Košice, Slovak Republic^f

¹⁹ School of Physics and Chemistry, University of Lancaster, Lancaster, UK^b

²⁰ Department of Physics, University of Liverpool, Liverpool, UK^b

²¹ Queen Mary and Westfield College, London, UK^b

²² Physics Department, University of Lund, Lund, Sweden^g

²³ Physics Department, University of Manchester, Manchester, UK^b

²⁴ CPPM, Université d'Aix-Marseille II, IN2P3-CNRS, Marseille, France

²⁵ Institute for Theoretical and Experimental Physics, Moscow, Russia

²⁶ Lebedev Physical Institute, Moscow, Russia^f

²⁷ Max-Planck-Institut für Physik, München, Germany^a

- ²⁸ LAL, Université de Paris-Sud, IN2P3-CNRS, Orsay, France
- ²⁹ LPNHE, Ecole Polytechnique, IN2P3-CNRS, Palaiseau, France
- ³⁰ LPNHE, Universités Paris VI and VII, IN2P3-CNRS, Paris, France
- ³¹ Institute of Physics, Czech Academy of Sciences, Praha, Czech Republic^{f,h}
- ³² Nuclear Center, Charles University, Praha, Czech Republic^{f,h}
- ³³ INFN Roma and Dipartimento di Fisica, Università "La Sapienza", Roma, Italy
- ³⁴ Paul Scherrer Institut, Villigen, Switzerland
- ³⁵ Fachbereich Physik, Bergische Universität Gesamthochschule Wuppertal, Wuppertal, Germany^a
- ³⁶ DESY, Institut für Hochenergiephysik, Zeuthen, Germany^a
- ³⁷ Institut für Teilchenphysik, ETH, Zürich, Switzerlandⁱ
- ³⁸ Physik-Institut der Universität Zürich, Zürich, Switzerlandⁱ
- ³⁹ Visitor from Yerevan Phys. Inst., Armenia
- ⁴⁰ On leave from LBL, Berkeley, USA
- ^a Supported by the Bundesministerium für Forschung und Technologie, FRG, under contract numbers 6AC17P, 6AC47P, 6DO57I, 6HH17P, 6HH27I, 6HD17I, 6HD27I, 6KI17P, 6MP17I, and 6WT87P
- ^b Supported by the UK Particle Physics and Astronomy Research Council, and formerly by the UK Science and Engineering Research Council
- ^c Supported by FNRS-NFWO, IISN-IIKW
- ^d Supported by the Polish State Committee for Scientific Research, grant nos. 115/E-743/SPUB/P03/109/95 and 2 P03B 244 08p01, and Stiftung für Deutsch-Polnische Zusammenarbeit, project no.506/92
- ^e Supported in part by USDOE grant DE F603 91ER40674
- ^f Supported by the Deutsche Forschungsgemeinschaft
- ^g Supported by the Swedish Natural Science Research Council
- ^h Supported by GA ČR, grant no. 202/93/2423, GA AV ČR, grant no. 19095 and GA UK, grant no. 342
- ⁱ Supported by the Swiss National Science Foundation

1 Introduction

The high center of mass (cms) energy of $\sqrt{s} \sim 300$ GeV available at the electron proton collider HERA has led to a renewed interest in the study of J/ψ production in lepton proton scattering. The production cross section is dominated by photoproduction, i.e. by the interaction of almost real photons, $Q^2 \approx 0$, where Q^2 is the negative four momentum transfer squared to the scattered lepton. The topic of this paper is an analysis of photoproduction of J/ψ mesons in *elastic* and *inelastic* processes.

Several mechanisms have been suggested to describe photoproduction of J/ψ mesons

$$\gamma p \rightarrow J/\psi X.$$

For the description of the *elastic* (or *exclusive*) process where $X = p$, a diffractive mechanism has been proposed by Donnachie and Landshoff [1]. The mechanism is based on Regge phenomenology where J/ψ production is mediated by pomeron exchange (Fig. 1(a)) and can be extended to include also *proton dissociation* (Fig. 1(b)). Measurements at HERA are expected to shed new light on the diffractive production mechanism and the nature of the pomeron [2]. At lower center of mass energies pomeron exchange was successfully used in the framework of the vector dominance model (VDM) [3, 4] to describe the production of *light* vector mesons. The predicted slow variation with energy of the elastic cross section was confirmed and an exponentially falling t distribution was found, where t is the squared four momentum transfer to the scattered proton. When applied to J/ψ meson production at low center of mass energies the prediction of the VDM model was found to be more than an order of magnitude above the data but other features like energy dependence and t distributions agreed within errors.

Attempts have been made to describe *elastic* J/ψ production in perturbative QCD. In the approach by Ryskin [5] the interaction between the proton and the charm quark is mediated by the exchange of a gluon ladder (Fig. 1(c)). Non perturbative effects are included in the gluon distribution of the proton which enters the production cross section quadratically. A measurement of elastic J/ψ production could therefore be a sensitive probe of the gluon density in the proton. Recently higher order effects have been calculated in this model and a comparison to preliminary HERA data [6] was carried out [7]. The Ryskin model predicts a different energy dependence of the elastic J/ψ cross section than the Donnachie-Landshoff approach. The energy dependence in the Ryskin model is coupled to the low x behaviour of the gluon density in the proton. Using a gluon density increasing towards low x which describes recent measurements of the structure function F_2 at HERA[8], results in a fast increase of the cross section for elastic photoproduction of J/ψ [7].

In *elastic* J/ψ production at small momentum transfer the J/ψ meson retains approximately the full photon energy ($z \approx 1$ with $z = E_\psi/E_\gamma$ in the proton rest system). J/ψ production *with proton dissociation* although strictly speaking an inelastic process also leads to z values close to 1. In contrast, *inelastic* processes will have z values below 1 and a high mass hadronic state is formed. The principal inelastic process proposed is the photon gluon fusion mechanism where the photon emitted by the incoming lepton interacts with a gluon from the proton via the charm quark (Fig. 1d). This mechanism is calculable in perturbative QCD due to the hard scale given by the mass of the charm quark. Attempts have been made to determine the gluon density in the proton from this reaction in several fixed target experiments [9, 10, 11]. In the colour singlet model [12] for photoproduction of J/ψ , which is based on this picture, the formation of a J/ψ state is accompanied by the emission of a hard gluon. Comparing predictions of the colour singlet model to data a discrepancy in absolute magnitude was found

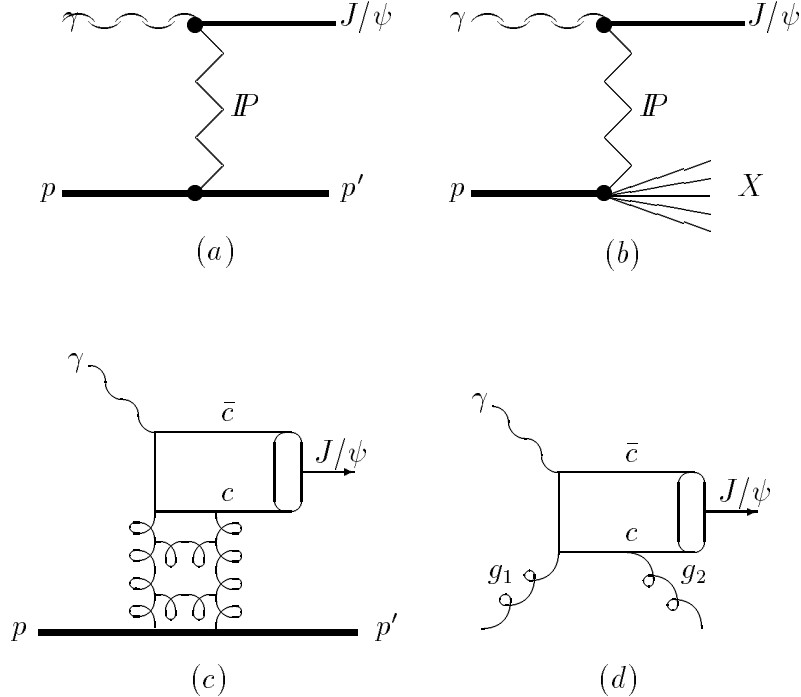


Figure 1: J/ψ production mechanisms: (a) elastic J/ψ production via pomeron exchange; (b) diffractive proton dissociation; (c) elastic J/ψ production in perturbative QCD: exchange of a gluon ladder [5]; (d) photon gluon fusion model for inelastic J/ψ production (colour singlet model [12]).

which was attributed to missing higher order calculations (“K-factor”). Subsequently several improvements have been proposed which led to better agreement with the data [13]. Recently, complete next-to-leading order (NLO) calculations have been performed [14, 15] and compared successfully to fixed target data and to preliminary HERA data.

Motivated by TEVATRON data on inelastic J/ψ and ψ' production [16] which may require colour octet contributions to explain the measured cross sections, calculations have been performed for possible colour octet contributions in photoproduction at HERA [17, 18]. Both groups attempt to estimate the colour octet contributions to J/ψ mesons at high z ; in [17] the contribution to *inelastic* J/ψ production is estimated.

We present here an analysis of elastic and inelastic J/ψ production in positron proton collisions near $Q^2 = 0$ for γp cms energies up to 150 GeV. The analysis is based on J/ψ decays to leptons, $J/\psi \rightarrow \mu^+\mu^-$ or $J/\psi \rightarrow e^+e^-$. The data were collected with the H1 detector at HERA and correspond to an integrated luminosity of $\sim 2.7 \text{ pb}^{-1}$.

The *inelastic* process is analysed for the first time in H1; preliminary results have also been shown by the ZEUS collaboration [6]. The analysis of the *elastic* process is an update of a previous letter [19] where we have presented a measurement of $\sigma(\gamma p \rightarrow J/\psi + X)$ which showed a strong increase of the cross section with $W_{\gamma p}$, the photon proton center of mass energy, compared to experiments at lower cms energy. This increase was faster than expected from the Donnachie-Landshoff prediction. At that time contributions from processes with proton dissociation could however not be excluded completely. With the increased statistics now available and an improved analysis method these inelastic processes can be efficiently recognised. The fast increase of the elastic cross section with $W_{\gamma p}$ was also observed by the ZEUS collaboration [20, 6].

The paper is organised as follows. After a brief introduction of the kinematics (section 2), the experimental conditions and the pre-selection of the data sample are described in section 3. The analysis of the *elastic* J/ψ samples follows in section 4, which includes the energy dependence of the total γp cross section and the distribution of p_t^2 , the transverse momentum of the J/ψ . The second part of section 4 contains the analysis of the *proton dissociation* process and the decay angle distribution of diffractively produced J/ψ mesons. In section 5 the selection of the inelastic events is discussed and results are presented including the energy dependence of the γp cross section, the distributions of p_t^2 and of the elasticity z of the J/ψ . A first cross section for ψ' production in the HERA energy range is given in the last section.

2 Kinematics

The variables used for the description of J/ψ photoproduction at HERA are:

$$Q^2 = -q^2 = -(k - k')^2 \quad (1)$$

$$t = (P_p - P')^2 \quad (2)$$

$$s = (P_p + k)^2 \quad (3)$$

$$y = \frac{P_p \cdot q}{P_p \cdot k} \quad (4)$$

$$W_{\gamma p} = \sqrt{(P_p + q)^2} \quad (5)$$

with the 4-momenta P_p and k of the incoming proton and positron, k' of the scattered positron, $q = k - k'$ of the exchanged photon, and P' of the system X, which is identical to the proton for elastic J/ψ production.

The Bjorken variable y can for photoproduction be approximated by $y \approx E_\gamma/E_e$, where E_γ and E_e are the energies of the exchanged photon and the incoming positron. The variable y can be computed from the observed final state using the method by Jacquet–Blondel [21]:

$$y = \frac{\Sigma (E - P_z)}{2E_e} = \frac{(E - P_z)_{J/\psi} + \Sigma_{\text{rest}}(E - P_z)}{2E_e}. \quad (6)$$

The sum is over all visible particles, i.e. tracks and energy deposits in the calorimeter. In order to avoid double counting the calorimeter energy in a cylinder of radius 30 cm around the extrapolated charged tracks is excluded. For events where only the two J/ψ decay leptons are observed in the tracking detector the calorimeter information is not used for the calculation of y . Analysing photoproduction it is customary to use $W_{\gamma p}$:

$$W_{\gamma p}^2 = y s - Q^2 + m_p^2 \approx y s$$

The separation of the events into an elastic and an inelastic sample utilizes the topology of the event and the variable z which is defined as:

$$z = \frac{P_p \cdot P_\psi}{P_p \cdot q} \quad (7)$$

where P_ψ is the four vector of the J/ψ . Using eqn. (4) z can be expressed as:

$$z = \frac{y_\psi}{y} \quad \text{with} \quad y_\psi = \frac{(E - P_z)_{J/\psi}}{2 E_e}, \quad (8)$$

For elastic events $y_\psi = y$ and thus $z = 1$.

The ep cross section and the γp cross section are related by:

$$\sigma(ep \rightarrow e J/\psi X) = \int_{y_{min}}^{y_{max}} dy \int_{Q_{min}^2(y)}^{Q_{max}^2} dQ^2 \cdot f_{\gamma/e}(y, Q^2) \cdot \sigma_{\gamma^*p}(Q^2, y) \quad (9)$$

where the cross section on the left side is the measured ep cross section covering a range $Q_{min}^2 \leq Q^2 \leq Q_{max}^2$ and determined in bins of y . The kinematical minimum for a given value of y is Q_{min}^2 , and Q_{max}^2 is the effective upper limit of the selected event samples:

$$Q_{min}^2 = m_e^2 \frac{y^2}{1-y}; \quad Q_{max}^2 = 4 \text{ GeV}^2.$$

The flux of *transverse* photons is [22]:

$$f_{\gamma/e}(y, Q^2) = \frac{\alpha}{2\pi} \frac{1}{y Q^2} \cdot \left(1 + (1-y)^2 - \frac{2m_e^2 y^2}{Q^2} \right).$$

The longitudinal photon flux amounts to 2% of the transverse flux for the given kinematical range. Since the photon flux decreases rapidly with Q^2 and y , the weak Q^2 and y dependences of $\sigma_{\gamma^*p}(Q^2, y)$ play only a minor role and the photoproduction cross section $\sigma(\gamma p \rightarrow J/\psi X)$ can in first approximation be identified with $\sigma_{\gamma^*p}(Q^2, y)$. It is then obtained as:

$$\sigma(\gamma p \rightarrow J/\psi X) = \sigma(ep \rightarrow e J/\psi X) / \Phi_{\gamma/e}$$

where $\Phi_{\gamma/e}$ is the photon flux integrated over Q^2 and y . The correction for this approximation is small; it can be taken into account as a small change of the $W_{\gamma p}$ value at which the cross section measurement is performed.

3 Experimental Conditions

The data were taken in 1994 with the H1 detector operating at the electron proton storage ring HERA, where positrons of 27.5 GeV collide with protons of 820 GeV. In 1994 HERA was operated with 153 colliding positron and proton bunches. The integrated luminosity used for this analysis is 2.7 pb^{-1} for the decay $J/\psi \rightarrow \mu^+ \mu^-$ and 2.0 pb^{-1} for $J/\psi \rightarrow e^+ e^-$. The H1 detector is described in [23]. We repeat here the essential features of the detector components used for the analysis.

3.1 The H1 Detector

The central tracking system is mounted concentrically around the beamline and covers polar angles¹ between 20° and 160° . Measurements of charge and momenta of charged particles are provided by two coaxial cylindrical drift chambers (central jet chambers, CJC) [24]. Two sets of cylindrical drift chambers for measurement of the z -coordinate and multiwire proportional chambers (MWPC) for triggering are placed at two radial positions. One set surrounds the beamline within the inner CJC and the other is mounted in between the two jet chambers. The central tracking system is complemented by a forward tracking system which covers polar angles $7^\circ \lesssim \theta \lesssim 25^\circ$. In the present analysis the forward tracker is only used to detect events with tracks other than the J/ψ decay leptons.

The tracking system is surrounded by a highly segmented liquid argon (LAr) sampling calorimeter [25] with an inner electromagnetic section consisting of lead absorber plates with a total depth of 20 to 30 radiation lengths and an outer hadronic section with steel absorber plates. Polar angles between 4° and 153° are covered by the calorimeter and the total depth is 4.5 to 8 interaction lengths depending on the polar angle. The backward region, $155^\circ \lesssim \theta \lesssim 176^\circ$, is covered by a lead scintillator calorimeter where the scattered positron is detected for $Q^2 \gtrsim 4 \text{ GeV}^2$. The magnetic field of 1.15 T is produced by a superconducting solenoid surrounding the LAr calorimeter.

The iron flux return yoke surrounding the superconducting solenoid is instrumented with limited streamer tubes to provide muon identification; it is segmented into 10 iron plates of 7.5 cm thickness and instrumented with up to 16 layers of streamer tubes. Muon tracks are reconstructed in the region $4^\circ \lesssim \theta \lesssim 171^\circ$ with a spatial resolution of the order of 1 cm.

In addition to this central muon detector there is a toroidal muon spectrometer outside the main H1 magnet covering small polar angles. In the present analysis its driftchambers which cover $3^\circ \lesssim \theta \lesssim 17^\circ$, are used for the recognition of events with proton dissociation. For the same purpose a system of scintillators – the proton tagger – is placed 24 m downstream the proton beam around the beampipe, covering an angular range of approximately $0.06^\circ \lesssim \theta \lesssim 0.25^\circ$.

The luminosity is measured using the radiative process $ep \rightarrow ep\gamma$ where the photon is detected in a luminosity monitor [26, 23].

3.2 Trigger and Data Processing

The background rate at HERA is high, mainly due to interactions of the beam protons with gas in the beam pipe or surrounding material and due to photoproduction of light quarks. Therefore a restrictive trigger is necessary which cannot use the distinctive signature of the scattered positron since for photoproduction the positron stays in the beampipe². The trigger essentially has to rely on the decay leptons of the J/ψ .

Compared to our previous report [19] the trigger for muons and for electrons from J/ψ decays has been improved resulting in an approximate efficiency for electron pairs of 50% and for muon pairs of nearly 60% with a tolerable background rate.

The following triggers are utilized:

¹H1 uses a right-handed coordinate system defined as follows: the origin is at the nominal interaction point with the z -axis pointing in the proton beam direction, hence the polar angle θ is measured with respect to the proton beam direction. The region of small polar angles is called “forward”. The plane perpendicular to the z axis is named $r - \phi$ plane.

²The scattered positron is with a few exceptions not detected in the low angle tagger, because there was practically no overlap of its sensitive region ($y \gtrsim 0.3$) with the bulk of the J/ψ data which are at $y \lesssim 0.25$.

1. **Track triggers from Multi Wire Proportional Chambers (MWPC)** [27] demanding the origin of the tracks in the z direction to be near the nominal vertex region.
2. A **coplanar track trigger** constructed from the MWPCs which demands exactly two tracks of transverse momentum $p_t \gtrsim 500$ MeV, roughly coplanar with the beams.
3. A **driftchamber track trigger** [28] demanding one track in the CJC with a transverse momentum $p_t > 450$ MeV which originates from the interaction point in the plane perpendicular to the beams within ~ 2 cm.
4. **Muon triggers** demanding a penetrating particle detected in the central muon systems.
5. A **calorimetric trigger** for low energy electromagnetic clusters with $E > 800$ MeV roughly aligned with a track candidate in the proportional chambers.

These triggers are combined such that each event class is triggered by at least two different trigger combinations which can be compared with each other for determination of the efficiency. For exclusive J/ψ meson production in both leptonic decay modes a combination of elements 1, 2 and 3 gives a trigger based purely on tracking chambers. A trigger for muons – which is used for elastic and inelastic processes – is based on track triggers 1 and 3 and the muon trigger 4. For electrons the combination of track triggers 1 and 3 with the calorimetric trigger 5 is used imposing a requirement of low track multiplicity in the MWPCs therefore only sensitive to elastic and proton dissociation processes.

3.3 Track Selection and Lepton Identification

The event selection starts from tracks found in the central drift chambers CJC which have been associated to the primary e^+p interaction point (vertex) in a constrained fit which helps to increase momentum resolution and to reduce pattern recognition ambiguities.

Electrons are identified in the electromagnetic section of the LAr Calorimeter by linking a reconstructed drift chamber track to a calorimeter cluster with energy $E_{cluster} > 0.8$ GeV and demanding the measured energy to be comparable with the momentum ($E_{cluster}/p_{track} > 0.7$). The efficiency for electron identification is $\approx 85\%$ for $p > 0.8$ GeV.

A particle is identified as a *muon* if the track in the drift chamber is either linked to a track element reconstructed in the central muon detector or if it is identified as a minimum ionizing particle in the LAr Calorimeter. For the link with a track in the central muon system a drift chamber track is extrapolated taking into account the deflection in the magnetic field, the energy loss in the material of the detector and multiple scattering. The χ^2 probability comparing the parameters of the two tracks is required to be above 1%. A muon signature in the LAr Calorimeter is defined by an energy deposit below 3 GeV around the extrapolated track, at least three active cells in the hadronic part of the calorimeter, and the particle has to penetrate at least 90 % of the calorimeter. With these requirements the thresholds are 0.8 GeV for the identification of muons in the LAr calorimeter ($\approx 75\%$ efficiency above ~ 1 GeV) and 1.5 GeV in the central muon system ($\approx 80\%$ efficiency above ~ 2 GeV).

3.4 Event Simulation and Efficiency Determination

Monte Carlo (MC) techniques are used in order to determine the geometrical acceptance, the trigger and selection efficiencies. Events are generated using models and the detector response is simulated in detail. The simulated events are subjected to the same reconstruction and analysis chain as the data.

Two models are used to simulate J/ψ production. Inelastic J/ψ production is simulated by the generator EPJPSI [29] which is based on the colour singlet model in leading order. Diffractive J/ψ production – elastic and proton dissociation – is modelled by the Monte Carlo generator DIFFVM [30].

Diffractive events are generated with an energy dependence proportional to $W_{\gamma p}^{0.9}$, an exponential t distribution $\sim \exp(-b|t|)$ with a fixed slope of $b = 4 \text{ GeV}^{-2}$ in the elastic mode and $b = 2 \text{ GeV}^{-2}$ for proton dissociation. The proton dissociation mode has an additional parameter, the mass M_X of the dissociated proton. Events are generated with a $1/M_X^2$ distribution for M_X^2 above 4 GeV^2 . Below 4 GeV^2 the distribution is closely modelled to diffractive proton dissociation data obtained from deuterium measurements [31]. The system X is fragmented at masses above 2 GeV by treating it as a system of quark and diquark and using the Lund string model [32]. Below 2 GeV it is treated as a nucleon resonance and decays into nucleon and pions according to the known branching ratios.

The detector response in the Monte Carlo simulation is checked in detail by comparing to the data. After applying small overall correction factors the dependence of the efficiencies for track reconstruction, particle identification and triggering on the polar angle and the momentum of the J/ψ decay particles is well described by the simulation. This tuned Monte Carlo simulation is then used for correcting the data and remaining differences between data and Monte Carlo are included in the systematic errors.

3.5 Pre-selection of the J/ψ Samples

Elastic and inelastic J/ψ events in general look quite different in the detector, elastic events having only the decay leptons measured while inelastic events are characterized by additional tracks. Initially a common selection aims to identify lepton pairs in the J/ψ mass region irrespective of any other activity in the detector. Two tracks are selected with a common origin at the beam interaction point in the $r - \phi$ plane and momenta above 0.8 GeV in the range of polar angles $20^\circ \leq \theta \leq 160^\circ$. Both tracks have to be identified as muons or electrons. The z -coordinate of the event vertex has to be within 40 cm of the average beam collision point.

For low multiplicity events, one of the main backgrounds is due to cosmic ray muons, which are efficiently rejected by demanding the angle between the lepton candidates to be less than 177° .

Photoproduction events are selected by requiring no scattered positron be visible in the calorimeter, i.e. below a polar angle of 176° . Rejecting energy clusters above 8 GeV restricts the photon virtuality to $Q^2 \lesssim 4 \text{ GeV}^2$.

4 Analysis of the Elastic and Proton Dissociation Processes

Starting from the pre-selected data a two track sample is selected for the determination of the cross section for elastic J/ψ production and for proton dissociation processes. The selected

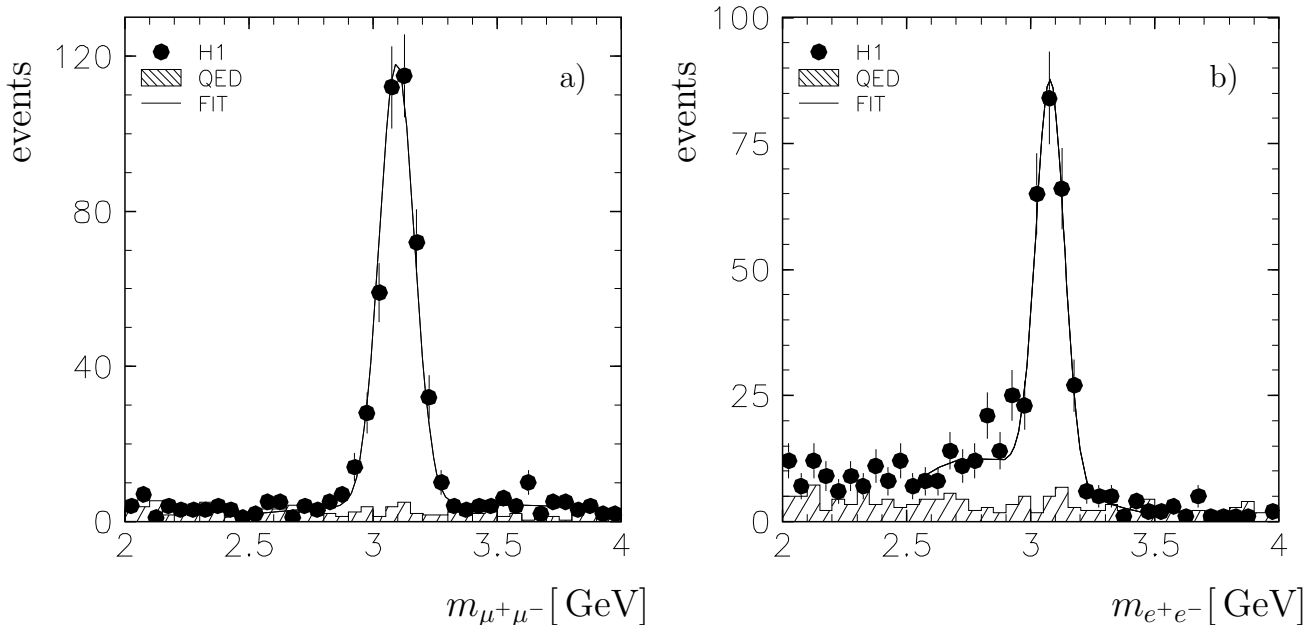


Figure 2: Mass distribution for $\mu^+\mu^-$ (a) and e^+e^- pairs (b) for the two track selection above 2 GeV. The curves are fits of a Gaussian plus a polynomial background to the J/ψ mass region. The shaded histogram shows the contribution of QED lepton pairs. For $\mu^+\mu^-$ the maximum of the fit is at (3.10 ± 0.01) GeV with a width of 76 MeV. For e^+e^- the maximum is at (3.08 ± 0.02) GeV and the width is 77 MeV. For both cases the detector simulation yields a width of 65 MeV.

lepton pairs are required to be the *only tracks* coming from the beam interaction point in the sensitive region of the tracking detectors ($7^\circ \lesssim \theta \lesssim 165^\circ$).

The reconstructed invariant mass of the lepton pairs for these events is shown in Fig. 2a) and b) for electrons and muons, respectively. A cut around the nominal mass $|m_{\ell^+\ell^-} - m_{\psi}| < 225$ MeV is applied. This yields about 400 (350) J/ψ candidates for muon (electron) pairs.

As can be seen from Fig. 2 the background below the J/ψ mass peak for this two track sample is low. It can be described by lepton pairs produced via a two photon process, where a photon is emitted by the incoming positron and by the proton. This process is calculable in QED. The calculation is implemented in the Monte Carlo generator LPAIR [33], the result of which is also shown in Fig. 2.

A subtraction is made for the background below the resonance, approximately 5% for $J/\psi \rightarrow \mu^+\mu^-$ and 12% for $J/\psi \rightarrow e^+e^-$. The number for electron pairs is larger because it contains two effects in addition to the QED lepton pairs. There is an additional background of misidentified hadrons with a decreasing mass spectrum which has to be subtracted; on the other hand there is a small loss of signal events due to the low mass tail of the J/ψ peak. The latter is due to radiation in the material of the detector according to the detector simulation.

At this stage the two track event sample is composed of elastic events and those with proton dissociation where the fragments of the excited proton are not visible in the tracking detector. The events are then classified into two samples, one *with* and one *without* activity in the forward detectors. The sample with forward activity will be used in section 4.2 to determine the cross section for J/ψ production with proton dissociation. For elastic J/ψ production the sample without signals in the forward detectors is used.

The forward detectors close to the proton beam (see section 3.1) are the proton tagger, the drift chambers of the forward muon spectrometer, and the low angle region of the liquid argon calorimeter ($4^\circ \lesssim \theta \lesssim 10^\circ$). They are sensitive to particles originating from secondary interactions of the excited nucleon fragments with material of collimators and the beampipe. Their efficiency has been studied with data [34].

The three detector systems have different thresholds as regards the mass M_X of the dissociated nucleon system X . The proton tagger is sensitive down to the lightest nucleon excitation, the forward muon detector is sensitive for $M_X \gtrsim 1.5$ GeV and the low angle region of the LAr calorimeter for $M_X \gtrsim 3$ GeV.

4.1 Elastic J/ψ Production

Monte Carlo studies show that after the two track selection, 85% of the events with proton dissociation are recognised in the forward detectors. The elastic event sample is selected by rejecting those events containing an energy deposit above 0.75 GeV in the forward LAr calorimeter, or having hits in the proton tagger or having more than one hit pair in the forward muon system. The event numbers are listed in table 1.

The remainder of the proton dissociation background is subtracted statistically using the Monte Carlo simulation program DIFFVM of J/ψ production with proton dissociation. The simulated events are normalized to the number of events with forward detector signal. All three forward detectors independently lead to the same normalization within errors. In table 1 the correction factor which is applied to account for remaining proton dissociation background is indicated in the line marked '1 - $f_{p.diss.}$ '.

Additional background from ψ' decays is removed taking into account the measured fraction of ψ'/ψ production of $\approx 20\%$ (see section 6) and applying the selection cuts to the simulated cascade decays into $J/\psi + anything$. A correction of $4 \pm 2\%$ is applied.

The remaining event sample has been examined by a visual scan in order to detect unrecognised background. A small number of events has energy deposits in the calorimeter which might indicate a background. This number is less than the background expected due to ψ' decays and no further correction is applied.

Cross section as function of $W_{\gamma p}$

The elastic ep cross section is evaluated in bins of $W_{\gamma p}$ in the range of 30 – 150 GeV. The Q^2 range is limited to $Q^2 \lesssim 4$ GeV² with an average of 0.13 GeV². The cross section was calculated according to:

$$\sigma_{ep} = \frac{N_{bg.corr.}(1 - f_{p.diss.})(1 - f_{\psi'})}{\epsilon_{sel} \epsilon_{trigger} \epsilon_{acc} \mathcal{L}}$$

where the factors are the number of events corrected for background below the mass peak $N_{bg.corr.}$, the background fractions of proton dissociation and ψ' $f_{p.diss.}$ and $f_{\psi'}$, respectively, the efficiencies for data selection ϵ_{sel} (including track reconstruction, selection cuts, and lepton identification) efficiency for triggering $\epsilon_{trigger}$, the geometrical acceptance ϵ_{acc} , and the integrated luminosity \mathcal{L} . The results for the ep cross section are given in table 1 taking into account the branching ratio for one leptonic decay channel of $(6.0 \pm 0.25)\%$. The ep cross section can be converted into a γp cross section using the relations of section 2. The integrated photon flux

$W_{\gamma p}$ [GeV]	30–60	60–90	90–120	120–150
$J/\psi \rightarrow \mu^+ \mu^-$				
events (bg. corrected)	52.0±7.5	64.0±8.6	80.0±10.0	37.0±6.6
ϵ_{acc}	0.512±0.020	0.844±0.034	0.669±0.027	0.390±0.016
$1 - f_{p.diss.}$	0.88±0.12	0.87±0.11	0.88±0.11	0.87 ±0.11
$\epsilon_{selection}$	0.486±0.039	0.396±0.032	0.485±0.039	0.581±0.046
$\epsilon_{trigger}$	0.371±0.030	0.490±0.039	0.724± 0.058	0.828±0.066
$\sigma(ep \rightarrow eJ/\psi p)$ [nb]	2.9±0.4±0.5	2.0±0.3±0.4	1.7±0.2±0.3	1.0±0.2±0.2
$J/\psi \rightarrow e^+ e^-$				
events (bg. corrected)	48.4±7.5	62.5±8.5	43.1±7.1	10.6±3.5
$\epsilon_{selection}$	0.550±0.038	0.515±0.036	0.447± 0.031	0.223±0.016
$\epsilon_{trigger}$	0.474±0.033	0.550±0.039	0.684± 0.048	0.791±0.055
$\sigma(ep \rightarrow eJ/\psi p)$ [nb]	2.5±0.4±0.4	1.8±0.2±0.3	1.5±0.2±0.3	1.1±0.3±0.2

Table 1: **Elastic J/ψ production:** Efficiencies and cross sections for elastic J/ψ production measured via the leptonic decays to $\mu^+ \mu^-$ and $e^+ e^-$ are given in intervals of $W_{\gamma p}$ ($Q^2 \lesssim 4$ GeV²) in the acceptance region. The number of events (two track selection requiring **no** forward tag) is corrected for background below the mass peak. The remaining proton dissociation background $f_{p.diss.}$ is calculated by Monte Carlo. The acceptance ϵ_{acc} describes the probability for both leptons to be in the θ range $20^\circ \leq \theta \leq 160^\circ$. The selection efficiency $\epsilon_{selection}$ contains the efficiencies for track reconstruction, lepton identification and selection cuts. The errors of acceptance, proton dissociation background, selection and trigger efficiency give the systematic errors. The first error of the ep cross section is statistical, the second one systematic.

$J/\psi \rightarrow l^+ l^-$				
$W_{\gamma p}$ [GeV]	30–60	60–90	90–120	120–150
W_0 [GeV]	42	72	102	132
$\Phi_{\gamma/e}$	0.0736	0.0370	0.0229	0.0149
$\sigma(\gamma p \rightarrow J/\psi p)^{\mu\mu}$ [nb]	39.6±5.7±7.2	53.4±7.2±9.8	76.2±9.5±13.9	67.3±11.9±12.3
$\sigma(\gamma p \rightarrow J/\psi p)^{ee}$ [nb]	34.4±5.3±6.0	48.2±6.6±8.4	63.8±10.4±11.1	71.0±23.4±12.4
$\sigma(\gamma p \rightarrow J/\psi p)$ [nb]	36.8±3.9±6.6	50.6±4.8±9.1	70.6±7.0±12.7	68.0±10.6±12.2
$\sigma(\gamma p \rightarrow J/\psi X)$ [nb]	23.0±3.2±4.0	63.5±5.8±11.4	62.7±7.4±11.2	128.9±19.5±23.2

Table 2: **Elastic J/ψ production and J/ψ production with proton dissociation:** γp cross sections for the elastic production of J/ψ mesons are given for decays to muons and electrons separately and also combined. In the last line the combined cross section for J/ψ production with proton dissociation is given. W_0 is the corrected bin center. $\Phi_{\gamma/e}$ is the photonflux integrated over Q^2 and $W_{\gamma p}$. The first error of the cross section is the statistical error, the second one systematic.

is shown in table 2. The center W_0 of the $W_{\gamma p}$ bins of 30 GeV width is calculated taking into account a y dependence of the γp cross section corresponding to $\sim W_{\gamma p}^{0.9}$, a Q^2 dependence of $\sigma_{\gamma^* p}$ as given by the VDM propagator $(m_\psi^2/(Q^2 + m_\psi^2))^2$, and the longitudinal cross section to be Q^2/m_ψ^2 times the transverse cross section. The difference to the uncorrected bin center is estimated to be -3 GeV.

Since the data based on J/ψ decays into $\mu^+\mu^-$ and e^+e^- agree within errors the γp cross sections have been averaged. The resulting combined cross section is shown in Fig. 3 and listed in table 2. The data show a rise with $W_{\gamma p}$ which in the HERA regime can be represented as $\sigma_{\gamma p} \propto W_{\gamma p}^\delta$. A fit to the H1 data yields $\delta = 0.64 \pm 0.13$, where the error includes statistics and systematic effects. In Fig. 3 also results by the ZEUS collaboration [20] in the same energy range as the present data are shown, which agree well. Using also the ZEUS data and the measurements at lower energies [35, 36, 37] which are also shown in Fig. 3, a combined fit yields $\delta = 0.90 \pm 0.06$.

The energy dependence expected from the Donnachie-Landshoff model [1] corresponds to $\delta = 0.32$ (neglecting any shrinkage, see also next section) and is also shown in Fig. 3. It falls below the HERA data by more than a factor of 3 corresponding to more than 3 standard deviations if normalised at fixed target energies.

The prediction of the QCD model due to Ryskin and including higher order corrections [7] is also compared with the data in Fig. 3. The prediction depends quadratically on the gluon distribution taken at the scale $(Q^2 + m_\psi^2)/4 \approx 2.4$ GeV², which can be parametrised as $x g(x) \propto x^{-\lambda}$ at low values of x , the fraction of the proton momentum carried by the gluon. For the present data $x \approx m_\psi^2/W_{\gamma p}^2 \approx 10^{-3}$. Using the gluon distribution function from MRSA' [38] corresponding to $\lambda \approx 0.2$, gives good agreement with the data between 10 and 150 GeV. The sensitivity to the gluon distribution is illustrated by comparison to the GRV fit [39] which corresponds to $\lambda \approx 0.3 - 0.4$. The corresponding curve in Fig. 3 with the parameters used in [7] yields a steeper energy dependence than the data.

Systematic errors

A breakdown of the systematic error of the cross sections in tables 1 and 2 is given in table 3. The main contribution to the systematic error of elastic and proton dissociation cross sections is due to the separation of these two event classes. The uncertainty is estimated to be 12% by varying the cuts on the three forward detectors and by using different combinations of two of them. The uncertainty of the background which was subtracted statistically in the elastic cross section was estimated to be 2% and is included in the total of 12%. It was estimated by varying the assumed $1/M_X^k$ dependence of the cross section from $k=2$ to $k=2.5$ ($k = 2.2 \pm 0.2$ was measured in [40]).

The systematic errors of the track reconstruction efficiency (3%), single muon identification (5%), electron identification (4%) and trigger efficiency (9% and 8% for muon and electron triggers) are estimated by comparing the Monte Carlo efficiencies with the efficiencies determined from the data and using remaining differences as error.

The systematic error of the angular acceptance depends mainly on the energy dependence of the γp cross section and is estimated by varying $\sigma_{\gamma p} \propto W_{\gamma p}^\delta$ between $0.6 \leq \delta \leq 1.0$ which results in a 4% error. The uncertainty in the background due to ψ' cascade decays via J/ψ accounts for the measurement error on the ratio of ψ'/ψ production. For the evaluation of the γp cross section an uncertainty in the photon flux of 2% is estimated by varying the upper limit of the Q^2 integration by ± 1 GeV.

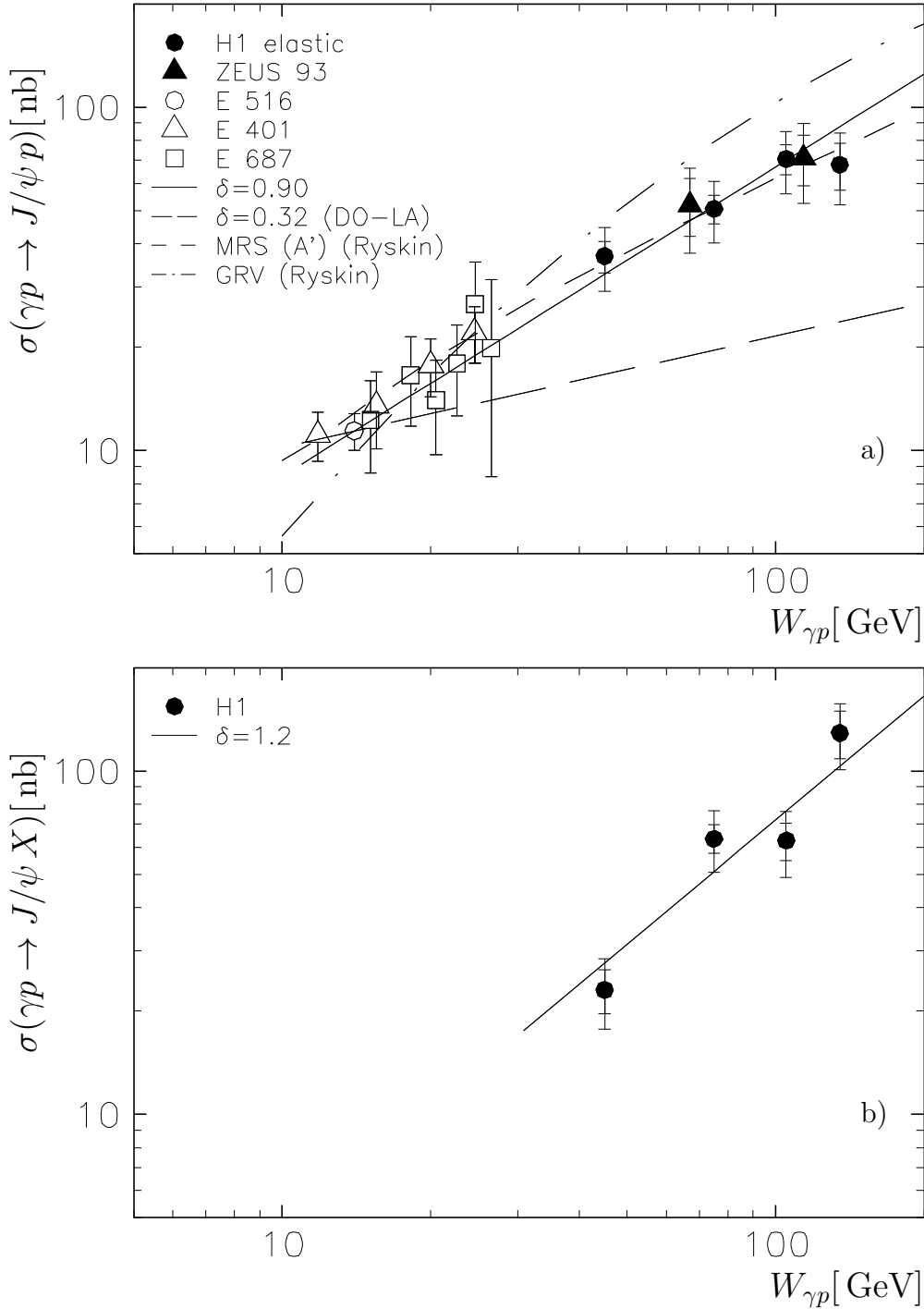


Figure 3: **a)** Total cross section for **elastic** J/ψ photoproduction. The inner error bars of the HERA points are statistical, the outer ones contain statistical and systematic errors added in quadrature. The data at lower cms energies are from previous experiments [35, 36, 37]; they were corrected with the new J/ψ decay branching ratio where necessary and include systematic errors (added in quadrature). A parametrisation of the energy dependence as $W_{\gamma p}^\delta$ with $\delta = 0.90$ (full curve) and $\delta = 0.32$ (long dashed) normalized to the E 516 point is shown. Also shown is the result of calculations according to the Ryskin model [7] using the MRSA' (dashed) and GRV parametrisations (dash dotted) of the gluon density. **b)** Total cross section for J/ψ -production with **proton dissociation**. The inner error bars of the H1 points are statistical, the outer ones contain statistical and systematic errors added in quadrature. The full line represents a fit to $W_{\gamma p}^\delta$ with $\delta = 1.2 \pm 0.2$.

	$\mu^+\mu^-$	e^+e^-
Separation elastic/p.diss.	12%	
Trigger	9%	8%
Single lepton identification	5%	4%
Single track reconstruction	3%	
Acceptance	4%	
Branching ratio	4%	
Photon flux	2%	
Luminosity	1.5%	
ψ' -background	2%	
Total	18 %	17%

Table 3: *Systematic errors*

p_t^2 distribution

The t -distribution is one of the distinctive features of a diffractive process. It is expected to be exponential and the slope parameter in Regge type models is expected to increase with energy (shrinkage) as $b = b_0 + 2\alpha' \ln W_{\gamma p}^2/W_0^2$ with $\alpha' = 0.25 \text{ GeV}^{-2}$ for pomeron exchange [1]. In contrast, models based on perturbative QCD predict little shrinkage.

Since the scattered electron is not measured, t can only be approximately determined for the data assuming $Q^2 = 0$, then $t \approx -p_t^2$ where p_t^2 is the transverse momentum of the J/ψ with respect to the beam axis. The data analysis was carried out as in the previous section, but the efficiencies and background proportions were determined in bins of p_t . The cross section $d\sigma_{ep}/dp_t^2$ is shown in Fig. 4 a. A steep slope is observed for $p_t^2 < 1 \text{ GeV}^2$ with a tail towards higher values. The tail is compatible with Monte Carlo expectations for events with $Q^2 \neq 0$.

The slope obtained by a log-likelihood-fit of an exponential $\exp(-bp_t^2)$ to the data below $p_t^2 \leq 1 \text{ GeV}^2$ is

$$b = (4.0 \pm 0.2 \pm 0.2) \text{ GeV}^{-2}.$$

The first error is statistical. The second one contains the dominant systematic contributions estimated by varying the upper limit of the fit region in p_t^2 between 0.75 and 1.25 GeV^2 or by using a χ^2 -fit, alternatively. The error in the slope parameter due to using p_t^2 instead of t is calculated in the simulation to be -10% .

For the $W_{\gamma p}$ range from 30 GeV to 90 GeV the fit yields $b = (3.7 \pm 0.3 \pm 0.2) \text{ GeV}^{-2}$ and $b = (4.5 \pm 0.4 \pm 0.3) \text{ GeV}^{-2}$ for the interval from 90 GeV to 150 GeV. Within the errors no clear evidence for shrinkage is observed. The expected change in the b slope from the Regge prediction is only 0.6 GeV^{-2} in the HERA energy range. This is of the same order of magnitude as the experimental errors, therefore no conclusion can be drawn with present statistics from the data in the HERA energy range alone.

The experimental situation at low cms energies is unclear: b -values ranging from $b \approx 3 \text{ GeV}^{-2}$ to $b \approx 5 \text{ GeV}^{-2}$ were measured [9, 10, 36, 41, 42] thus also preventing any conclusion about shrinkage.

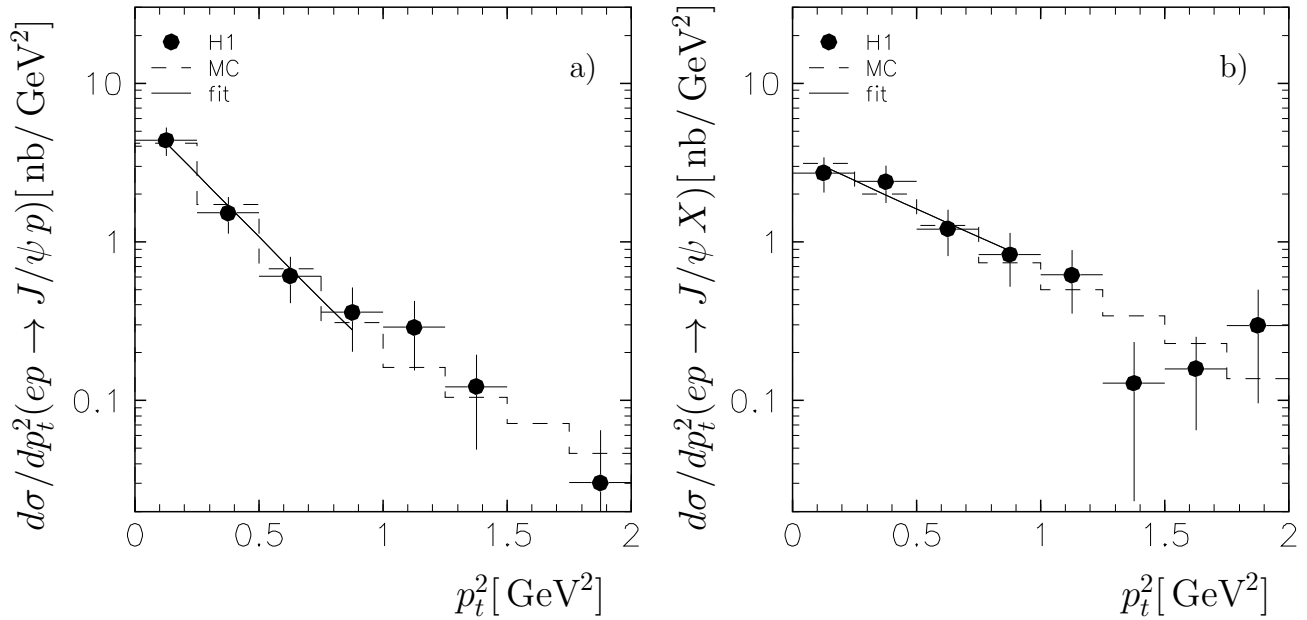


Figure 4: **a)** $d\sigma/dp_t^2$ for **elastic** J/ψ production integrated over $30 \text{ GeV} \leq W_{\gamma p} \leq 150 \text{ GeV}$. The error bars contain statistical and systematic errors added in quadrature. The straight line is a fit to the data in the range $p_t^2 \leq 1 \text{ GeV}^2$ of the form $\exp(-bp_t^2)$ with $b = 4.0 \pm 0.3 \text{ GeV}^{-2}$. The histogram shows the p_t^2 distribution of the DIFFVM Monte Carlo. **b)** $d\sigma_{\gamma p}/dp_t^2$ for J/ψ meson production with **proton dissociation** integrated over $30 \text{ GeV} \leq W_{\gamma p} \leq 150 \text{ GeV}$. The straight line is an exponential fit to the data in the range $p_t^2 \leq 1 \text{ GeV}^2$ which yields a value of $b = 1.6 \pm 0.3 \text{ GeV}^{-2}$, the dashed line represents the DIFFVM Monte Carlo calculation.

4.2 J/ψ Production with Proton Dissociation

Energy dependence and p_t^2 distribution

For the measurement of the proton dissociation cross section the two track sample *with* a signal in one of the forward detectors is used as defined in section 4. The Monte Carlo generator DIFFVM for proton dissociation with parameters as in section 3.4 is used for acceptance and efficiency determination. The procedure for calculating the cross section and systematic errors is the same as in the elastic case. The main contribution to the systematic error is due to the selection of the event sample with the help of the forward detectors. The size of the error is essentially the same (12%) since both cross sections, the elastic and the proton dissociation cross section, are nearly of the same magnitude. The systematic error of the acceptance may be slightly larger than in the elastic case due to uncertainties in the M_X dependence, this is however not taken into account.

The γp cross section for J/ψ production with proton dissociation derived from J/ψ decays to $\mu^+\mu^-$ and e^+e^- as a function of $W_{\gamma p}$ is given in table 2 and shown in Fig. 3b. It can be fitted by a $W_{\gamma p}^\delta$ dependence with $\delta = 1.2 \pm 0.2$ (statistical and systematic error), slightly larger than the value for the elastic data, which may be explained by the increased phase space for producing excited nucleon systems at higher energy.

The cross section $d\sigma_{ep}/dp_t^2$ for J/ψ production with proton dissociation is shown in Fig. 4 b. A log-likelihood fit below 1 GeV^2 gives:

$$b = (1.6 \pm 0.3 \pm 0.1) \text{ GeV}^{-2}.$$

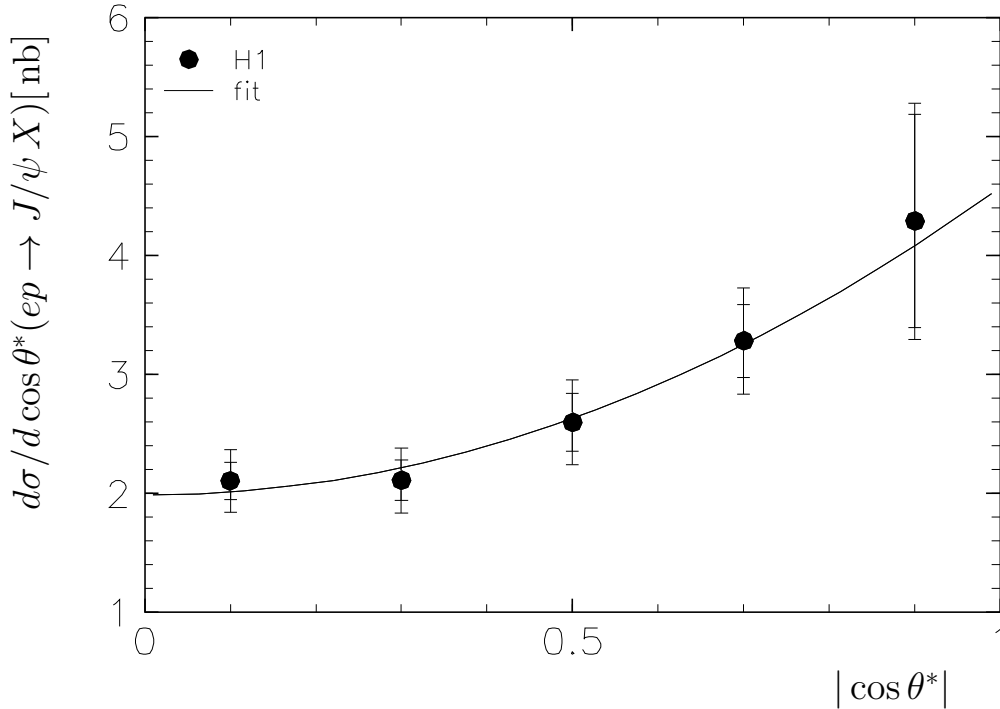


Figure 5: $d\sigma/d\cos\theta^*$ for diffractive J/ψ production (elastic and proton dissociation). The inner error bars are statistical, the outer ones contain statistical and systematic errors added in quadrature. The curve is a fit of the form $\propto (1 + \text{const} \cos^2 \theta^*)$.

The first error is statistical while the second one represents the systematic error estimated as in the elastic case. The error in the slope parameter due to using p_t^2 instead of t is calculated in the simulation to be -6.5% . The slope parameter is roughly a factor 2 smaller than for pure elastic scattering.

Decay angular distribution

The polarisation of the J/ψ can be accessed via the angular distribution of the J/ψ decay leptons. The angle θ^* is used, which is the angle in the J/ψ rest frame, between the direction of the positively charged decay lepton and the J/ψ direction in the γp cms (helicity frame) [4, 43]. Assuming s-channel helicity conservation the expected angular distribution is:

$$\frac{d\sigma}{d\cos\theta^*} \propto (1 - \rho) \sin^2 \theta^* + \rho \frac{1 + \cos^2 \theta^*}{2}$$

where ρ , the fraction of transversely polarised J/ψ mesons, is predicted to be one.

The ep cross section for both decay channels $J/\psi \rightarrow \mu^+\mu^-$ and $J/\psi \rightarrow e^+e^-$ as a function of $\cos\theta^*$ is shown in Fig. 5. The full two track sample is used in this analysis including elastic and proton dissociation samples. A χ^2 fit yields $\rho = 1.2 \pm 0.2$, which is consistent with s-channel helicity conservation.

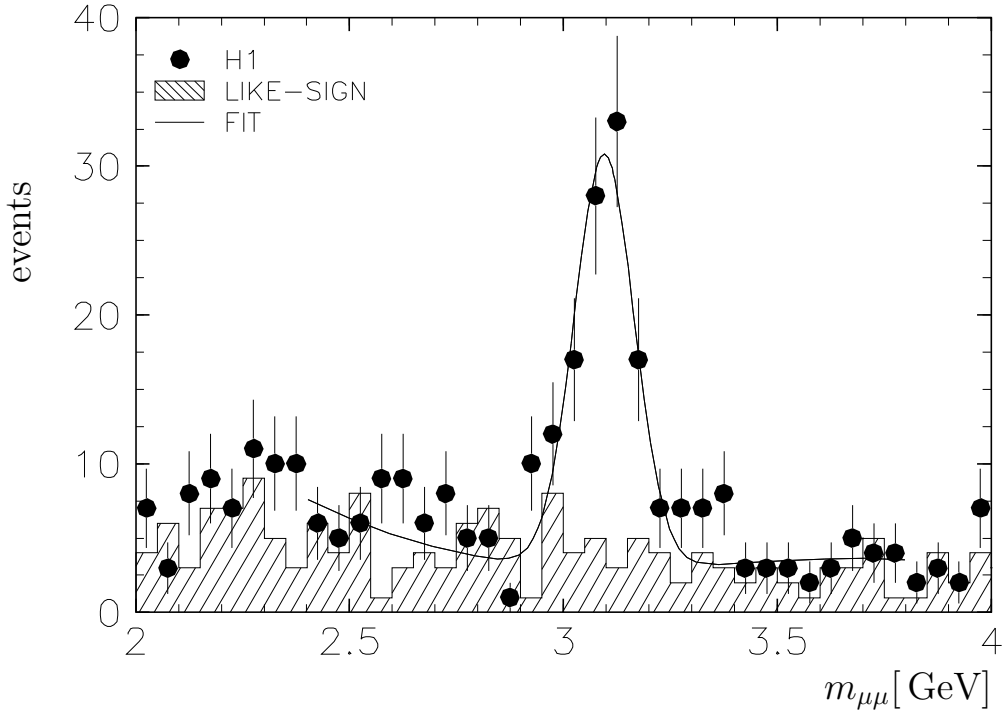


Figure 6: Mass distribution for $\mu^+\mu^-$ of the **inelastic** event sample. The curve is a fit of a Gaussian plus a polynomial background to the J/ψ mass region. The shaded histogram shows the mass distribution of like sign muon pairs. The maximum of the fit is at (3.10 ± 0.01) GeV with a width of 65 MeV.

5 Inelastic J/ψ Production

The event selection for inelastic J/ψ production starts from the preselected lepton pair sample described in section 3.5. The mass distribution for $\mu^+\mu^-$ pairs with at least one additional track from the interaction point is shown in Fig. 6. The inelastic J/ψ candidates are selected by a cut around the nominal mass of ± 225 MeV. The background is due to muons from leptonic π and K decays and misidentified hadrons. It is subtracted by using the data above and below the mass peak as an estimate of the background.

The elasticity z – calculated according to eqn. 8 in section 2 – is used to define the inelastic sample. In Fig. 7 an overview over *all* candidates for $J/\psi \rightarrow \mu^+\mu^-$ is shown as function of z . The measured z distribution is shown for the inelastic J/ψ candidates with $z > 0.3$. The total two track sample and also the subsample with activity in the forward detectors which were used in the previous section to evaluate the elastic and proton dissociation cross sections, respectively, are shown in the highest z -bin of the figure. The data in Fig. 7 are compared with three Monte Carlo models: the contribution of photon gluon fusion as modelled in the generator EPJPSI (LO colour singlet model) is shown, at high z the contribution of proton dissociation processes as modelled in DIFFVM can be seen, and at low z the contribution of the hadronic component of the photon, the “resolved photon process [44]”, is shown as modelled by EPJPSI. Note that the simulations are normalized to the data. DIFFVM with proton dissociation is normalised to the two track data with forward detector signal. The contribution of photon gluon fusion is normalised to the inelastic data for $0.45 < z < 0.90$ and the resolved component is multiplied by the same normalisation factor.

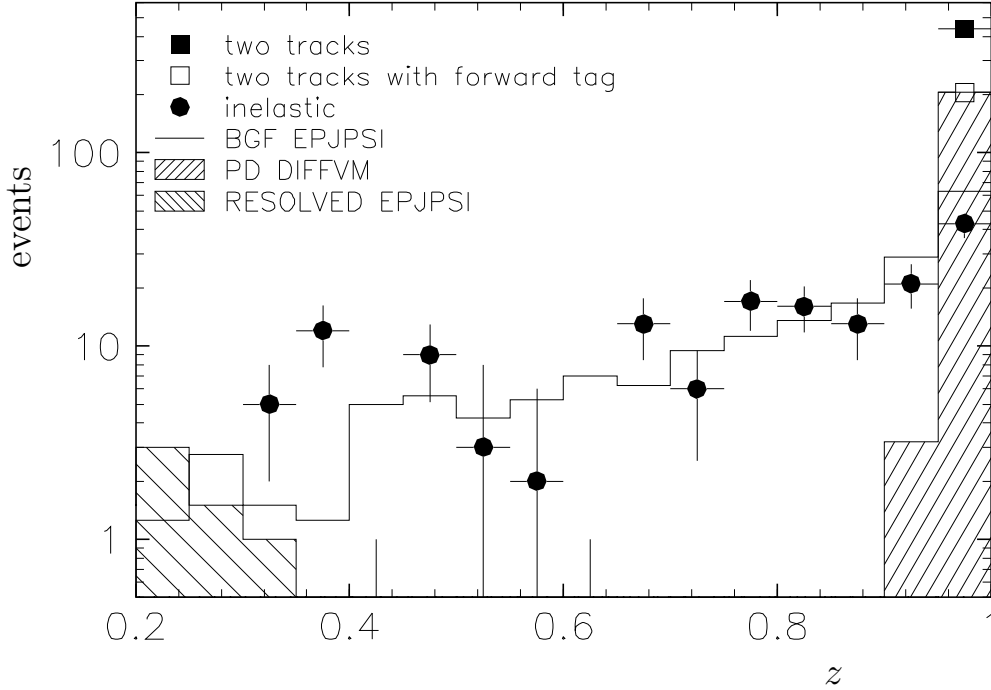


Figure 7: Distribution of the elasticity z for $J/\psi \rightarrow \mu^+\mu^-$. The H1 data in the J/ψ mass window are corrected for background below the mass peak. They are classified as events with exactly two tracks irrespective of any forward tag (full square), events with exactly two tracks and a forward tag (open square) and inelastic events with $z > 0.3$ (full circle). For comparison the following model calculations are shown: a diffractive model including proton dissociation (DIFFVM) normalized to the data (two tracks with forward tag); a LO photon gluon fusion model (LO BGF EPJPSI) for inelastic J/ψ production using the gluon distribution from the MRSD-’ parametrisation, and the resolved contribution calculated in EPJPSI with the GRV-LO photon structure function. The resolved contribution is scaled with the same normalisation factor as the contribution from photon gluon fusion.

An inelastic sample is selected by requiring $0.45 \leq z \leq 0.90$ which rejects diffractive and resolved photon events and yields a total of ≈ 100 J/ψ candidates. The data sample is corrected for efficiency and acceptance using the Monte Carlo generator EPJPSI [29] with the parametrisation of the gluon density of MRSD-’ [45]. The cross section for inelastic J/ψ production is determined for $0 \leq z \leq 0.90$ in order to compare with theory. Therefore a correction is applied for the loss below $z < 0.45$, which is estimated to $13.5 \pm 2\%$, where the error is due to using a different gluon distribution (MRSD0’). An additional correction takes into account the contamination by J/ψ meson production via the resolved photon process. This background is estimated using an option of the Monte Carlo generator EPJPSI. Using the GRV-LO-parametrisation [46] of the photon structure function yields a background estimate of 2.5% for $z > 0.45$. The contribution changes by +2% using as photon structure function the parametrisation of LAC1 [47].

Systematic errors for trigger and selection efficiency are estimated as in the elastic analysis. In addition to the relevant errors quoted in table 3 which yield a contribution of 12%, a contribution to the systematic error of 10% is estimated specifically for the inelastic cross section. This number contains the uncertainty due to background subtraction, an error of the contamination

$J/\psi \rightarrow \mu^+ \mu^-$				
$W_{\gamma p}$ [GeV]	30–60	60–90	90–120	120–150
events (bg. corrected)	8.0 ± 3.7	27.0 ± 6.1	23.0 ± 8.3	27.0 ± 7.8
ϵ_{acc}	0.326 ± 0.013	0.799 ± 0.032	0.854 ± 0.034	0.731 ± 0.029
$\epsilon_{analysis}$	0.333 ± 0.027	0.387 ± 0.031	0.329 ± 0.026	0.279 ± 0.022
$\epsilon_{trigger}$	0.304 ± 0.024	0.290 ± 0.023	0.413 ± 0.033	0.646 ± 0.052
$\sigma(ep \rightarrow eJ/\psi X)$ [nb]	$1.5 \pm 0.7 \pm 0.2$	$1.8 \pm 0.4 \pm 0.3$	$1.2 \pm 0.4 \pm 0.2$	$1.3 \pm 0.4 \pm 0.2$
$\Phi_{\gamma/e}$	0.0736	0.0370	0.0229	0.0149
$\sigma(\gamma p \rightarrow J/\psi X)$ [nb]	$20.0 \pm 9.4 \pm 3.2$	$49.5 \pm 11.1 \pm 7.9$	$52.6 \pm 19.0 \pm 8.4$	$84.1 \pm 24.3 \pm 13.4$

Table 4: **Inelastic J/ψ production:** Efficiencies and cross sections for inelastic $J/\psi \rightarrow \mu^+ \mu^-$ production with $0 < z < 0.90$. The number of events is background corrected. $\Phi_{\gamma/e}$ is the photon flux integrated over Q^2 and $W_{\gamma p}$. The errors of acceptance, analysis and trigger efficiency are statistical and systematic errors added in quadrature. The first error of the cross sections is statistical, the second is systematic.

with resolved events, the correction for the low z region. A further contribution to the error of 5% is due to a systematic shift in the z determination after reconstruction. In the simulation z is found to be systematically shifted to higher values after reconstruction with respect to the generated value by 4% for $z = 0.8$ and by 10% for $z = 0.5$.

Energy dependence of γp cross section

The γp cross section for inelastic J/ψ production can be derived in a similar way as in section 4.1. Efficiencies, event numbers and the final cross section for $z < 0.9$ are given in table 4. The resulting γp cross section is shown in Fig. 8a. The data are compared to calculations in the colour singlet model including NLO contributions [15].

As input the theoretical calculations use the charm mass $m_c = 1.4$ GeV, $\Lambda_{\overline{MS}} = 300$ MeV, the renormalisation scale is chosen to be identical to the factorisation scale, $\sqrt{2} m_c$. Predictions are shown for different gluon density distributions that have been derived from recent data. The gluon distributions differ in the low x behaviour where x is the fraction of the proton momentum carried by the gluon. The distributions used can at low x be parametrised as $x g(x) \propto x^{-\lambda}$, and the values for λ range between 0 (MRSD0') [45]) and 0.4 (MRSG [38]). In Fig. 8a the curves contain an additional contribution of inelastic ψ' production ($\approx 15\%$, estimated in [15]). They reproduce approximately the energy behaviour of the data, but cover a wide range in absolute normalisation. The agreement with the data becomes better with increasing steepness of the gluon density at low x .

The NLO calculation is not fully under control for $p_t^2 \rightarrow 0$ and $z \rightarrow 1$ [48]. Missing contributions of even higher order cause problems as can be seen in Fig. 9 where the theoretical p_t^2 distribution bends over for $p_t^2 \lesssim 1$ GeV².

Therefore the data and prediction are shown in Fig. 8b for a restricted kinematical range, $z < 0.8$ and $p_t^2 > 1$ GeV² and thus requiring the emitted gluon to be hard (thereby reducing the data sample by a factor 2). Improved agreement is observed with all gluon density distributions but the sensitivity is reduced.

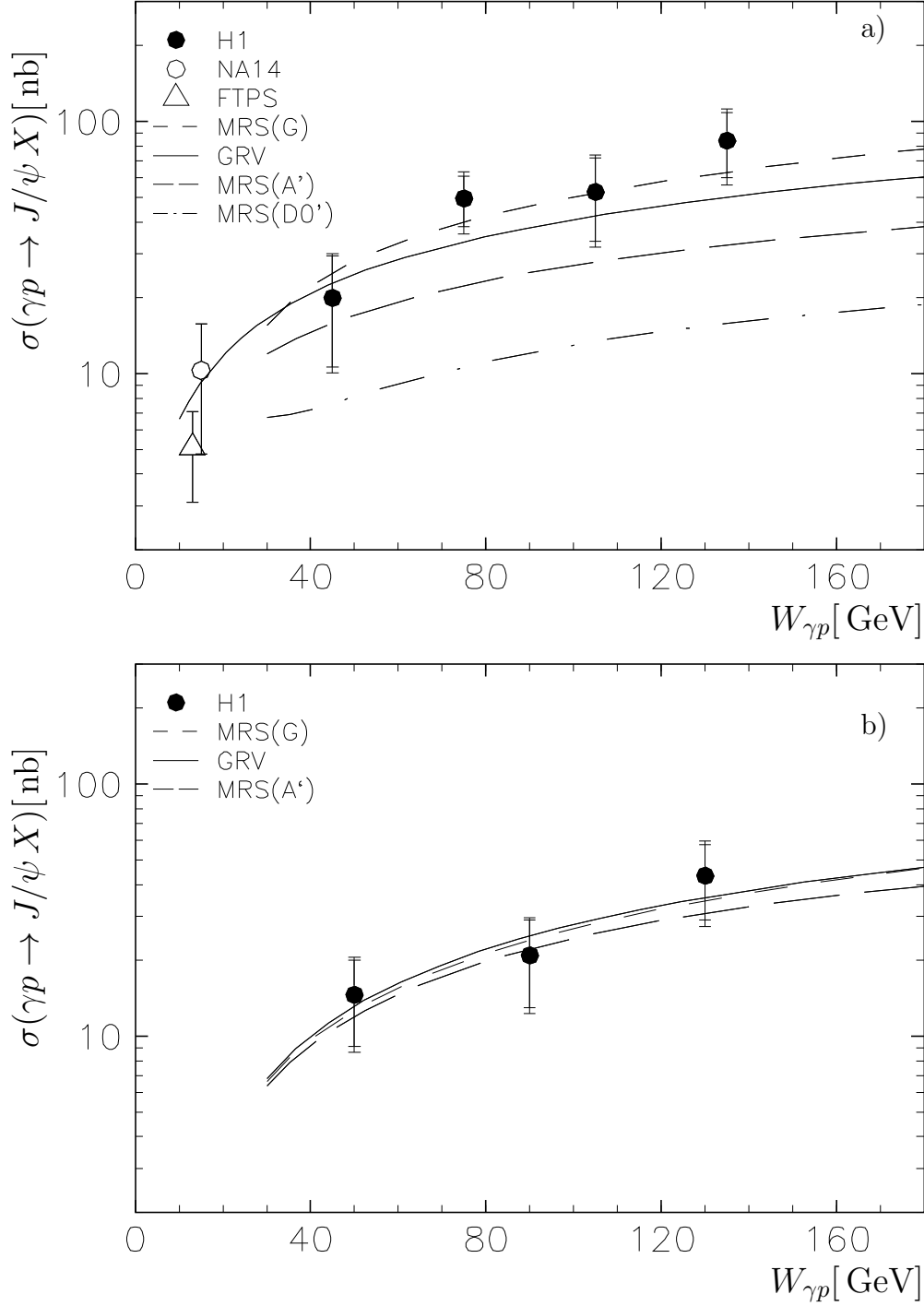


Figure 8: Total cross section for **inelastic** J/ψ -production for $z < 0.9$ (a) and $z < 0.8$ and $p_t^2 > 1 \text{ GeV}^2$ (b). The inner error bars of the H1 points are statistical, the outer include statistical and systematic errors added in quadrature. The curves represent NLO calculations [15] for different gluon distributions and contain a 15% correction taking into account ψ' background.

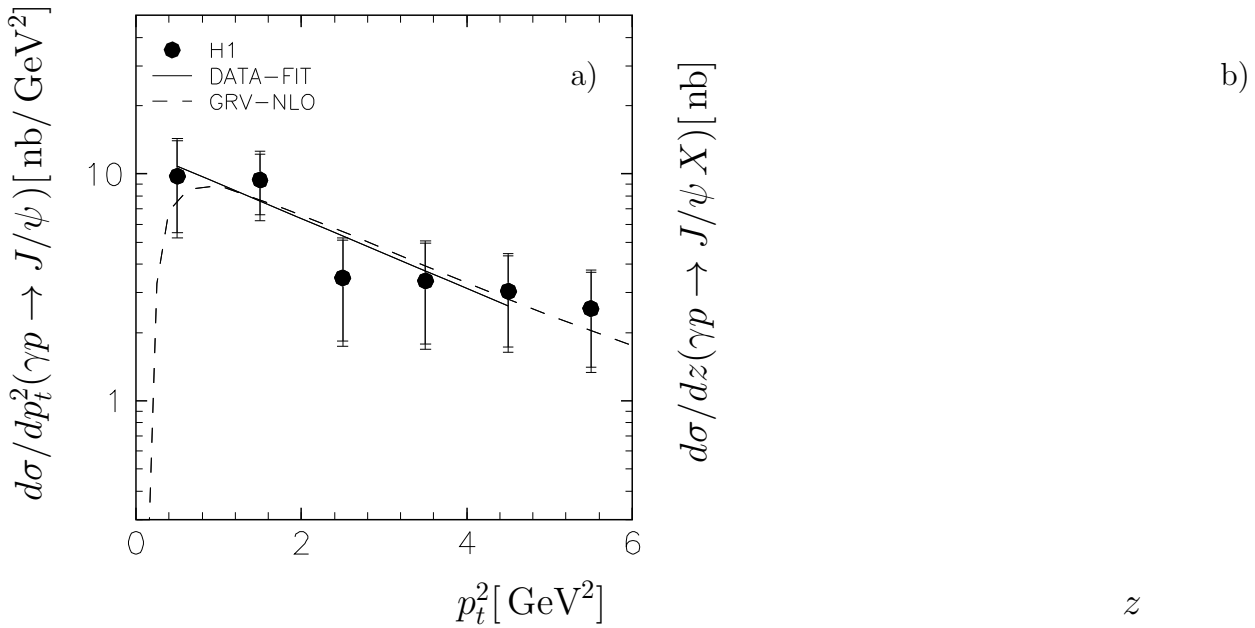


Figure 9: a) $d\sigma_{\gamma p}/dp_t^2$ for **inelastic** J/ψ production with $z < 0.9$ integrated over $30 \text{ GeV} \leq W_{\gamma p} \leq 150 \text{ GeV}$. The straight line is an exponential fit to the data in the range $p_t^2 \leq 5 \text{ GeV}^2$, the dashed line is a NLO calculation [15] at $W_{\gamma p} = 100 \text{ GeV}$ with the GRV structure function. b) $d\sigma_{\gamma p}/dz$ for inelastic J/ψ production with a cut $p_t^2 \geq 1 \text{ GeV}^2$, in comparison with NLO calculations in the colour singlet model with the GRV structure function. The LO colour octet calculation is from [17].

p_t^2 , z -distribution

In Fig. 9a the distribution of the transverse momentum p_t^2 of the J/ψ is shown for $z < 0.9$. A log-likelihood fit to the data of an exponential $\exp(-b p_t^2)$ in the region $p_t^2 \leq 5 \text{ GeV}^2$ yields:

$$b = (0.39 \pm 0.06 \pm 0.03) \text{ GeV}^{-2}$$

where the first error is statistical and where the systematical error is estimated by using a χ^2 -fit and varying the fit region. This result is in agreement with the NLO-calculation [15] which predicts a slope of $b = 0.3 \text{ GeV}^{-2}$ above a $p_t^2 > 1 \text{ GeV}^2$.

The differential energy distribution of the J/ψ , $d\sigma/dz$, is shown in Fig.9b with a cut in $p_t^2 > 1 \text{ GeV}^2$. It is compared with the NLO calculation [15] in the colour singlet model with the GRV [39] structure function for the proton. Agreement in shape and normalisation is found within errors. This is interesting in view of the speculations about possible additional colour octet contributions to photoproduction of J/ψ . These yield a large inelastic contribution at $z > 0.8$ [17] after fixing the normalisation by the CDF data[16]. The strong increase indicated in Fig. 9b is not supported by the present data.

6 ψ' Production

The same data sample as for the J/ψ analysis is used to measure the cross section for the diffractive photoproduction of ψ' mesons ($\psi(2S)$), by searching for the decay $\psi' \rightarrow J/\psi \pi^+ \pi^-$, where the J/ψ subsequently decays to a muon pair.

For this investigation, only the muon triggers are utilised, but the identification of the muon pair is otherwise identical to that used in the J/ψ analysis. It is further required that, in addition to the muon pair, exactly two other, oppositely charged tracks are found in the central tracking detector which are assumed to be pions. For events in which both pion candidates are measured in the central tracking detector to have a transverse momentum greater than 150 MeV, a mass difference is formed, defined as $\Delta M = m_{\mu^+\mu^-\pi^+\pi^-} - m_{\mu^+\mu^-}$. A peak of 7 events is found in an interval of ± 60 MeV around the mass difference, $\Delta M = m_{\psi'} - m_{J/\psi}$, with no background events seen outside the peak.

Monte Carlo studies show that this selection restricts the kinematic domain of acceptance to $z' > 0.95$, $40 \text{ GeV} < W_{\gamma p} < 160 \text{ GeV}$ and $Q^2 < 4 \text{ GeV}^2$, where $z' = E_{\psi'}/E_\gamma$ in the proton rest frame. The acceptance is estimated using the same Monte Carlo generator as was used for the J/ψ analysis, with parameters of the model chosen to match the J/ψ data. A mixture of elastic and proton dissociation events is assumed, which is compatible with that found in the J/ψ events. No separation of elastic events from events with proton dissociation is attempted. In the kinematic region above, the combined acceptance of trigger and selection is found to be $4.4 \pm 0.9\%$. Assuming a branching ratio for this ψ' decay of 0.019 ± 0.002 [49], the ep cross section for the production of ψ' in the kinematic domain $z' > 0.95$, $40 \text{ GeV} < W_{\gamma p} < 160 \text{ GeV}$ and $Q^2 < 4 \text{ GeV}^2$ is $2.9 \pm 1.1 \pm 0.6 \text{ nb}$, where the first error given is statistical, the second systematic. This translates into a photoproduction cross section, $\sigma_{\gamma p}(W_{\gamma p} = 80 \text{ GeV}) = 24 \pm 9 \pm 5 \text{ nb}$ for ψ' production with $z' > 0.95$ and $Q^2 < 4 \text{ GeV}^2$. The corresponding cross section for J/ψ production is the diffractive cross section (including elastic and proton dissociation) which at $W_{\gamma p} = 80 \text{ GeV}$ is $\sigma_{\gamma p} = 119.5 \pm 11.2 \pm 12.0 \text{ nb}$. The ratio of ψ' to J/ψ production is then 0.20 ± 0.09 which is in agreement with previous measurements [9, 41, 50].

7 Summary

J/ψ meson production in the photoproduction limit is analysed in the elastic channel. Corrections for contributions from events with proton dissociation are applied almost entirely on an event to event basis. The following results are found:

- The total γp cross section is observed to increase with energy as $W_{\gamma p}^\delta$ with $\delta = 0.64 \pm 0.13$ for H1 data alone, and $\delta = 0.90 \pm 0.06$ including the ZEUS and low energy data. This increase is faster than predicted in soft diffractive models ($\delta = 0.32$).
- A calculation using the model by Ryskin in the framework of perturbative QCD results in a good description of the energy dependence if the gluon distribution from the set MRSA' is used.
- The p_t^2 distribution of the elastic J/ψ data below 1 GeV^2 can be fitted with an exponential $e^{-bp_t^2}$, $b = 4.0 \pm 0.2 \pm 0.2 \text{ GeV}^{-2}$.

The γp cross section for J/ψ meson production with proton dissociation was determined. The γp cross section is as large as the elastic one and its energy dependence is slightly steeper than the elastic cross section, $\delta = 1.2 \pm 0.2$. The p_t^2 distribution is flatter than for the elastic process. The slope parameter is approximately a factor 2 smaller than for elastic data.

The angular distribution in the helicity frame was determined for the complete diffractive data sample, i.e. including elastic and proton dissociation contributions. The distribution in the

helicity frame is consistent with s-channel helicity conservation, $\rho = 1.2 \pm 0.2$, where ρ is the fraction of transversely polarised J/ψ mesons.

Inelastic J/ψ meson production can be described well by a QCD calculation in NLO of the colour singlet model if cuts are used which demand the emitted gluon to be hard, $p_t > 1$ GeV and $z < 0.8$, in order to make perturbation theory applicable. The agreement is observed in the shape of the $W_{\gamma p}$, p_t^2 and z distributions. The absolute normalization between data and theory agrees within the experimental errors of $\approx 30\%$, using any gluon distribution function which describes the F_2 data at low x . A comparison to the relative energy distribution z of inelastic J/ψ production with $p_t^2 > 1$ GeV² calculated in a colour octet model shows disagreement at high values and makes a large colour octet contribution unlikely.

Diffraction production of ψ' was observed. An estimate of the ratio of the cross section to the one for J/ψ yields 0.20 ± 0.09 in agreement with previous measurements at lower energy.

Acknowledgements

We are very grateful to the HERA machine group whose outstanding efforts made this experiment possible. We acknowledge the support of the DESY technical staff. We appreciate the big effort of the engineers and technicians who constructed and maintained the detector. We thank the funding agencies for financial support of this experiment. We wish to thank the DESY directorate for the support and hospitality extended to the non-DESY members of the collaboration. We wish to thank M. Krämer from the DESY theory group for many enlightening discussions and good collaboration. Thanks to R. Roberts (RAL) for providing us with his numerical results for elastic J/ψ production.

References

- [1] A. Donnachie and P.V. Landshoff, *Phys. Lett.* B348 (1995) 213; *ibid.* B296 (1992) 227.
- [2] P.V. Landshoff, The Two Pomerons, preprint hep-ph-9410250, Proceedings of the Summer School on Hadronic Aspects of Collider Physics, Editor M.P. Locher, Zuoz, Switzerland, August 1994.
- [3] J.J. Sakurai, *Ann. Phys.(NY)* 11 (1960) 1
M. Gell-Mann, F. Zachariasen, *Phys. Rev.* 124 (1961) 953
- [4] T.H. Bauer, R.D. Spital, D.R. Yennie, F.M. Pipkin, *Rev. Mod. Phys.* 50 (1978) 261 (1978)
S.D. Holmes, W. Lee, J.E. Wiss, *Ann. Rev. Nucl. Part. Sci.* 35 (1985) 397
- [5] M.G. Ryskin, *Z. Phys.* C57 (1993) 89
- [6] Contributions to the Int. Europhys. Conf. on HEP, Brussels, 1995:
H1 Coll., *Photoproduction of J/ψ Mesons at HERA*, EPS-0468
ZEUS Coll., *Elastic J/ψ Photoproduction at HERA* EPS-0386
ZEUS Coll., *Inelastic J/ψ Photoproduction at HERA* EPS-0387

- [7] M.G. Ryskin, R.G. Roberts, A.D. Martin and E.M. Levin preprint DTP/95/96 CBPF-NF-079/95, RAL-TR-95-065, hep-ph/9511228 (1995), revised February 1996
- [8] T. Ahmed et al., H1 Collaboration, *Nucl. Phys.* B439 (1995) 471
M. Derrick et al., ZEUS Collaboration, *Z. Phys.* C65 (1995) 379
- [9] J.J. Aubert et al. EMC Collaboration, *Nucl. Phys.* B213 (1983) 1
- [10] Ashman et al., EMC Collaboration, *Z. Phys.* C56 (1992) 21
- [11] Allasia et al., NMC Collaboration, *Phys. Lett.* B258 (1991) 493
- [12] E.L. Berger, D. Jones, *Phys. Rev.* D23 (1981) 1521
R. Baier and R. Rückl, *Nucl. Phys.* B201 (1982) 1
- [13] H. Jung, D. Krücker, C. Greub, D. Wyler, *Z. Phys.* C60 (1993) 721
- [14] M. Krämer, J. Zunft, J. Steegborn, P.M. Zerwas, *Phys.Lett.* B348 (1995) 657
- [15] M. Krämer, *Nucl. Phys.* B459 (1996) 3
- [16] CDF Coll, FERMILAB-CONF-94-136-E, June 1994, contribution to the XXVII International Conference on High Energy Physics, Editors P.J. Bussey and I.G. Knowles, Glasgow, Scotland, July 1994
CDF Coll, FERMILAB-CONF-95-226-E, July 1995, submitted to the Int. Symp. on Lepton Photon Interactions, Beijing 1995
D0 Coll., FERMILAB-PUB-96-003-E, January 1996
- [17] M. Cacciari and M. Krämer, DESY preprint DESY 96-005, 1995
- [18] J. Amundson, S. Fleming, I. Maksymyk, preprint UTTG-10-95, MADPH-95-914, hep-ph-9410250
- [19] H1 Coll., T. Ahmed et al., *Phys. Lett.* B338 (1994) 507
- [20] M. Derrick et al., ZEUS Coll., *Phys. Lett.* B350 (1995) 120.
- [21] F. Jacquet, A. Blondel, DESY 79-48 (1979) 391
- [22] V.M. Budnev et al., *Phys. Rep.* C15 (1975) 181
- [23] I. Abt et al., H1 Collaboration, DESY preprint DESY 93-103 (1993)
- [24] J. Bürger et al., *Nucl. Instr. and Methods* A279 (1989) 217
- [25] B. Andrieu et al., *Nucl. Instr. and Methods* A336 (1993) 460
- [26] S. Aid et al., H1 Coll., *Z. Phys.* C69 (1995) 27
T. Ahmed et al., H1 Coll., *Z. Phys.* C66 (1995) 529
- [27] S. Eichenberger et al., *Nucl. Instr. and Methods* A323 (1992) 532
- [28] Th. Wolff et al., *Nucl. Instr. and Methods* A323 (1992) 537

- [29] H. Jung, EPJPSI 2.0 in “Physics at HERA”, Proceeding of the Workshop, vol. 3 (1991) 1488
- [30] B. List, Diploma Thesis, Techn. Univ. Berlin, unpubl. (1993)
- [31] K. Goulianos, *Phys. Rep.* 101 (1983) 169
- [32] T. Sjöstrand, *Comp. Phys. Comm.* 39 (1986) 347, *ibid* 43 (1987) 367
- [33] S. Baranov et al., LPAIR – A generator for Lepton Pair Production in “Physics at HERA”, Proceeding of the Workshop, vol. 3 (1991) 1478
- [34] T. Jansen, Thesis, Univ. Hamburg, unpubl. (1995)
- [35] P.L. Frabetti et al., E687 Collaboration, *Phys. Lett.* B316 (1993) 197
- [36] M. Binkley et al., E401 Collaboration, *Phys. Rev. Lett.* 48 (1982) 73
- [37] B.H. Denby et al., FTPS Collaboration, *Phys. Rev. Lett.* 52 (1984) 795
- [38] A.D. Martin, R.G. Roberts and W.J. Stirling, *Phys. Lett.* B354 (1995) 155
- [39] M.Glück, E.Reya and A.Vogt, *Z. Phys.* C67 (1995) 433
- [40] F.Abe et al., CDF Collaboration, *Phys. Rev.* D50 (1994) 5535
- [41] R. Barate et al., NA-14 Collaboration, *Z. Phys.* C33 (1987) 505
- [42] M. Arneodo et al., NMC Collaboration, *Phys. Lett.* B332 (1994) 195
- [43] K. Schilling and G. Wolf, *Nucl. Phys.* B61 (1973) 381
- [44] H. Jung, G.A. Schuler and J. Terron, *Int. Journ. Mod. Phys.* A32 (1992) 7955
- [45] A.D. Martin, W.J. Stirling, and R.G. Roberts, *Phys. Lett.* B306 (1993) 145, *ibid.* B309 (1993) 492
- [46] M. Glück, E. Reya and A. Vogt, *Phys. Rev.* D46 (1992) 1973
- [47] A. Levy, H. Abramowicz and K. Charchula, *Phys. Lett* B269 (1991) 458
- [48] M. Krämer, private communication
- [49] L. Montanet et al., Particle Data Group, *Phys. Rev.* D50 (1994) 1173
- [50] M. Binkley et al., E401 Collaboration, *Phys. Rev. Lett.* 50 (1983) 302